Biotechnology and Bioprocess Engineering **2004**, 9: 428-434

A Proposal for Optical Diagnostics Through the Enhancement of Diffraction Patterns Using Thin-film Interference Filters

Carmen-Gabriela Stefanita* and YunFeng Shao

University of Alberta, Department of Electrical and Computer Engineering Edmonton, Alberta T6G 2V4, Canada

Abstract Coarse clumping of solid materials within diseased biological cells can have a marked influence on the light scattering pattern. Perturbations in refractive index lead to distinct variations in the cytometric signature, especially apparent over wide scattering angles. The large dynamic range of scattering intensities restricts collection of data to narrow angular intervals believed to have the highest potential for medical diagnosis. We propose the use of an interference filter to reduce the dynamic range. Selective attenuation of scattering intensity levels is expected to allow simultaneous data collection over a wide angular interval. The calculated angular transmittance of a commercial shortwave-pass filter of cut-off wavelength 580 nm indicates significant attenuation of scattering peaks below ~10°, and reasonable peak equalization at higher angles. For the three-dimensional calculation of laser light scattered by cells we use a spectral method code that models cells as spatially varying dielectrics, stationary in time. However, we perform preliminary experimental testing with the interference filter on polystyrene microspheres instead of biological cells. A microfluidic toolkit is used for the manipulation of the microspheres. The paper intends to illustrate the principle of a light scattering detection system incorporating an interference filter for selective attenuation of scattering peaks.

Keywords: interference filter, light scattering, microfluidic toolkit, spectral method

INTRODUCTION

Nanoscale probing of intracellular matter promises to offer reliable diagnostic procedures for biological cells [1]. Although monitoring biomolecular processes within a single living cell is still under investigation, the rapidly expanding field of nanobiotechnology has contributed to our understanding of subcellular mechanisms and architecture [1]. Among techniques capable of resolving morphological differences at the subcellular level, those based on measuring scattered light properties can provide a valuable means to distinguish between healthy and diseased cells. Experimental observations indicate that the cellular nucleus is responsible for low angle scattering [2]. Concurrently, the idea was advanced that organelles could be responsible for scattering at larger angles [2]. Light scattering experiments involving combinations of sub and multi-wavelength sized particles [3] have confirmed these findings: Sharp intensity peaks at low angles are followed by a fast decline in intensity with increasing angle when the particle size is large compared to light wavelength [3]. Subsequent addition of particles with sizes comparable to or smaller than the wavelength alters scattering intensities at larger angles [3].

Computational techniques such as finite-difference-time-domain (FDTD) [4,5] can take into account fluctuations in refractive index within a cell, therefore revealing the dependence of light scattering patterns on cellular biochemical and morphological structure. The nucleus was observed to be a significant scatterer, especially when its size increases relative to the rest of the cell throughout neoplastic progression [4]. FDTD simulations also revealed that nucleus size determines intensity levels of scattered light at small angles (up to 5° for a 15 μm cell), whereas the refractive index structure of the nucleus influences higher angle scattering (over 20°) [4]. Cells modeled with homogeneous nuclei do not display significant changes in high angle scattering with increased nuclear size. On the other hand, a heterogeneous nucleus gives rise to increased high angle scattering with increasing nuclear size [4].

The fact that scattering patterns reveal substantial information over a wide angular interval has important implications for clinical measurements. However, the large dynamic range of scattering intensities poses challenges for data collection. Optical techniques such as [6] detect only the maximum value of the scattered intensity. In other cases, *e.g.* [7] sampling is limited to the solid angle spanned by the detector. Gaining a better understanding of the internal structure and organization of a biological cell underscores the necessity of cytometric data collec-

***Corresponding author**
Present address: Virginia Commonwealth University, Department of Electrical Engineering, 601 W Main Street, P.O. Box 843072, Richmond, Virginia 23284-3072, USA
Tel: +1-804-827-7040 ext. 611 Fax: +1-804-828-4269
e-mail: cstefanita@vcu.edu

tion over the whole scattering regime. We propose the use of an interference filter to selectively attenuate scattering intensities. By suppressing intensity levels at smaller angles we avoid saturating the camera, allowing higher angles of scattering to be imaged. The latter need to display similar levels in intensity to be imaged concomitantly. Therefore, a good filter should perform reasonable peak equalization for angles higher than 10°. The calculated angular transmittance of a commercial shortwave-pass filter indicates that this filter type might be a useful starting point toward a more optimal design. We illustrate the principle of a light scattering detection system incorporating such a filter.

Due to large computational requirements for the FDTD technique, we employ an alternative method for calculating light scattering from cells. A simplified mathematical model of light propagation is used in conjunction with the spectral algorithm [8]. Biological cells are modeled as time-independent spatially inhomogeneous dielectrics [9,10]. This method has been previously used to study the physics of laser-plasma interactions [11], and has been subsequently adapted to light scattering by biological cells [9,10]. In this paper, we consider only scattering patterns of homogeneous objects. Although the light scattering detection system we are developing is ultimately intended for inhomogeneous biological cells, preliminary testing is performed on homogeneous polystyrene microspheres.

A microfluidic toolkit (μTK) instrument (Micralyne Inc., Edmonton, AB, Canada) [12] is used for the manipulation of the microspheres employed in this experiment. Microchannels of ~50 μm width, contained in a glass microchip are filled with a buffer solution. The injected diluted suspension of the sample to be tested is manipulated along the microchannels using high voltages. When a sphere or cell passes the detection area, a signal is recorded. The μTK was designed with a laser-induced fluorescence detection system, and is primarily employed for biological samples. However, in this experiment the μTK is used only to bring a microsphere to a certain point in the microchannel, in the illumination field of a laser. Detection occurs without fluorescence, by recording scattered photons incident on a charge-coupled device (CCD) camera incorporating an interference filter.

THEORETICAL MODEL

Scattering from a Single Cell

When light interacts with a cell, variations in refractive index give rise to a spatial light scattering distribution of varying intensity levels. The code we employed for calculating this spatial light scattering distribution is based on the spectral algorithm [8,9]. The model allows us to regard biological cells as inhomogeneous perturbations of the dielectric constant, where inhomogeneities on a scale length smaller than the wavelength are treated as sharp boundaries. The full set of Maxwell equations in three spatial dimensions is reduced to the following wave equation for the electric field amplitude:

$$\frac{\mu\varepsilon}{c^2}\frac{\partial^2}{\partial t^2}\vec{E} - \nabla^2\vec{E} + \nabla(div\vec{E}) = 0 \tag{1}$$

where μ and ε are the magnetic permeability and dielectric constant of the medium. Enveloping Eq. (1) with respect to time [9] reduces the order of the time derivative:

$$2i\frac{\omega_o}{c^2}\varepsilon\mu\frac{\partial\vec{E}}{\partial t} + \nabla^2\vec{E} + \frac{\omega_o^2}{c^2}\varepsilon\mu\vec{E} - \nabla(div\vec{E}) = 0 \tag{2}$$

If the scattering medium is inhomogeneous in the x-y plane and the electromagnetic wave is s-polarized, the last term of the left side in Eq. (2) is zero. One obtains a scalar wave equation with a two dimensional Laplacian:

$$2i\frac{\omega_o}{c^2}\varepsilon\mu\frac{\partial E}{\partial t} + \nabla^2 E + \frac{\omega_o^2}{c^2}\varepsilon\mu E = 0 \tag{3}$$

The scalar field approximation can also be considered in three spatial dimensions, with three spatial components for the Laplacian.

The magnetic permeability of a biological cell is assumed equal to 1. The dielectric constant is taken as the sum of two terms: $\varepsilon = \varepsilon_0 + \Delta\varepsilon(x,y,z)$, where ε_0 is the dielectric constant of the fluid outside the cell, considered homogeneous. The second term, $\Delta\varepsilon(x,y,z)$ accounts for perturbations in the dielectric constant due to the cytoplasm and the nucleus. These perturbations are assumed small in this model, $|\Delta\varepsilon| << \varepsilon_0$. The scattering medium is considered stationary. Taking into account the expression for ε, the scalar wave Eq. (3) can be rewritten as

$$2i\frac{\omega_o}{c^2}\varepsilon_o\frac{\partial E}{\partial t} + \nabla^2 E + \frac{\omega_o^2}{c^2}\varepsilon_o E = -\frac{\omega_o^2}{c^2}\Delta\varepsilon E \tag{4}$$

The left side accounts for the electromagnetic field propagation in a homogeneous medium, and the right side describes the interaction with inhomogeneous perturbations. The scalar wave Eq. (4) is solved in a three-dimensional region, with dimensions of the simulation box taken as a multiple of incident light wavelength. Further details on how the spectral method is applied are given in [9,10]. The strength of the code lies in its ability to significantly reduce computational requirements, thereby producing rapid scattering intensity estimates.

Results of the simulations were compared with linear perturbation theory and Mie scattering [9,10]. In the former case, the analytical stationary solution to Eq. (4) was obtained by the linear perturbation method. The scalar wave Eq. (4) was considered only in two spatial dimensions, and the time derivative term was neglected in the stationary regime. Employing a paraxial approximation [9] in Eq. (4), thereby assuming small-angle scattering, and expanding the electric field amplitude into an incident field amplitude E_0 and a scattered light amplitude δE (where $|\delta E| << |E_0|$), Eq. (4) takes the following form in the first order, with respect to perturbations δE and $\Delta\varepsilon$:

$$2ik_m \frac{\partial \delta E}{\partial x} + \frac{\partial^2 \delta E}{\partial y^2} + \frac{\omega_o^2}{c^2} \Delta \varepsilon E_o = 0 \quad (5)$$

$k_m = (\omega_o/c)\sqrt{\varepsilon_o}$ is the laser wavevector in the fluid outside the cell. Light scattering from square perturbations was considered to test the spectral algorithm solution. Fig. 2 in [9] illustrates this comparison, considering a refractive index of the medium of $n_o = \sqrt{\varepsilon_o} = 1.35$, and refractive index perturbations $\Delta n_o = 0.02$ (cytoplasm) and $\Delta n_n = 0.04$ (nucleus). This choice of refractive indices is consistent with parameters used in [13].

On the other hand, the validity of our code was also tested within the framework of Mie theory [14], considering the diffraction of a plane monochromatic wave by a homogeneous sphere. Mie theory provides a rigorous solution to Maxwell's equations for all components of the electromagnetic field in three spatial dimensions, taking into account boundary conditions on a spherical surface. Fig. 3 in [9] illustrates the comparison between Mie theory and three dimensional spectral method simulation results. Good agreement is achieved for scattering angles up to 25°. This happens despite the fact that the numerical model solves the wave equation for only one spatial component of the electric field, whereas Mie theory solves the full vector set of Maxwell's equations. The scalar wave approximation is valid in this angular range because the longitudinal component of the electric field $\vec{E}$ is small and $div\vec{E}$ is small for small-angle scattering, allowing us to neglect the last term on the left side of the full wave Eq. (2).

Filtering Scattered Light

In the early stages of the project we consider only forward scattered light, more precisely the region encompassing the largest intensity variation: 0° to 35°. The term 'light scattering pattern' defines the plot of the scattered light - in photons/(s·sr) - versus angle. More precisely, for a fixed azimuth angle φ, the angular distribution of the scattered light will undergo a series of maxima and minima with polar angle θ. Only a small fraction of the incident light is scattered. Fig. 1 shows a prediction of photon counts for different polar angles, considering scattering from a single cell with diameter 11 μm, not containing a nucleus. The refractive index of the cell was taken as 1.35, as it is a typical value for cytoplasm [15]. The refractive index of the medium was chosen as 1.30 to simulate biological tissue [16]. The first maximum close to the axis of incidence (up to ~1°) represents the unscattered light that goes through the cell. Beyond this first maximum, intensity levels decline sharply with scattering angle. We use the term figure of merit (FOM) to express the intensity level of the brightest peak (excepting the unscattered light peak below ~1°) with respect to the weakest peak (at 35°). The FOM of approximately 3-seen in the light scattering pattern of Fig. 1 - restricts the acquisition of cytometry data to reduced angular ranges.

Intensity levels at higher angles are too weak to be recorded simultaneously with strong low angle intensities.

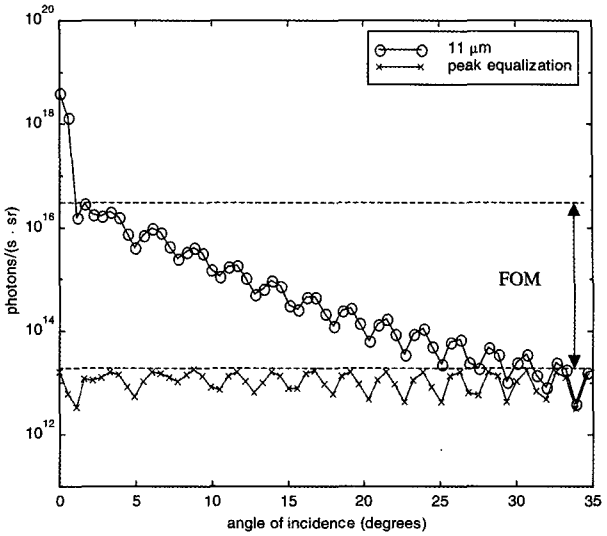

Fig. 1. Far-field distributions of scattered light from an 11 μm diameter cell (refractive index 1.35, medium 1.30). Equalization of scattering peak intensities obtained using an ideal filter. Gaussian beam of full-width-half-maximum (FWHM) = $20\lambda_0$ and wavelength λ_0 = 632.8 nm.

To ensure adequate contrast between rapidly decaying intensity levels, the scattered light needs to be selectively attenuated. Ideally, we want all scattering peaks to be of equal height. Fig. 1 illustrates an ideal distribution of photons/(s·sr) obtained by selectively attenuating scattering intensities for the 11 μm cell. The peak at 35° was used as a reference. If we want to be able to record its intensity level, all scattering peaks before 35° should display similar intensity values. We calculated the necessary transmittance for each peak that would reduce the height of the peaks, equalizing intensity levels. However, a commercially available filter that would perform such an ideal scattering peak equalization was not identified. Alternatively, we considered a filter that would at least significantly reduce low angle scattering intensities, while simultaneously equalizing intensity levels at higher angles The discussion for the choice of an appropriate filter is too long to be included in the present paper. We therefore highlight only a few steps, leaving the details and corresponding graphs for another paper [17].

Interference filters are usually designed for certain regions of the light spectrum. There is a relationship between the spectral and angular transmittance of an interference filter [18], based on

$$\lambda = \frac{\lambda_0 \sqrt{n^2 - \sin^2 \theta}}{n} \quad (6)$$

λ is the wavelength at off-normal angle θ, the central wavelength λ_0 corresponds to normal incidence, and n is the effective refractive index of the filter.

Although it is only approximate, such an angle-wavelength conversion can give a reasonable estimate for the angular transmittance of an interference filter. Based

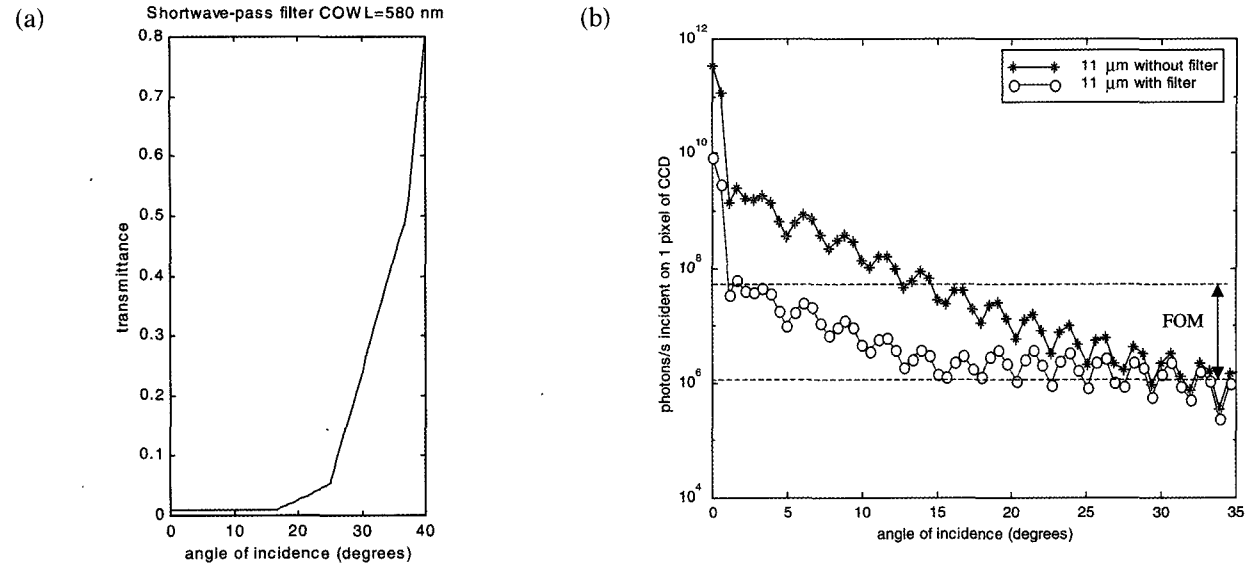

Fig. 2. a) Estimated angular transmittance of a shortwave-pass filter with cut-off wavelelength 580 nm. b) Spectral method calculations of photons/s incident on 1 pixel of CCD with and without a 580 nm shortwave-pass filter. Cell diameter 11 μm and laser wavelength 632.8 nm. Refractive indices: surrounding medium 1.30, cell 1.35 (no nucleus, only cytoplasm). Gaussian beam of FWHM = $20\lambda_0$.

on the transmittance values that would equalize scattering peaks, we were able to obtain the spectral transmittance of an equivalent filter [17]. Using the theory of light propagation through optical multilayers [19], we designed several interference filters, including shortwave-pass and bandpass. The optical properties displayed through the angular transmittance of a shortwave-pass filter of approximate cut-off wavelength (COWL) 595 nm indicated that this filter might be appropriate for our application [17]. Given the tolerances in manufacturing [17,18], the closest commercial counterparts for such a filter are shortwave-pass filters with COWL= 580 nm and 600 nm (Coherent Inc., Santa Clara, CA, USA). Using the spectral transmittance properties as indicated in the manufacturer's catalogue (Coherent Inc., Santa Clara, CA, USA), and applying the angle-wavelength conversion, Fig. 2a shows the estimated angular transmittance for the 580 nm filter. Fig. 2b illustrates the calculated angular distribution of scattered photons/s incident on 1 pixel of a Starlight-Xpress HX 516 camera, with and without a 580 nm filter. Although scattering peaks at smaller angles are attenuated significantly, their intensity levels are still higher than those of peaks at higher angles. This is due to the transmission properties of shortwave-pass filters. Nevertheless, scattering peaks above ~10° display intensity levels of similar height, indicating that they may be recorded simultaneously by the CCD camera. Overall, the FOM has been reduced to less than 2.

Instrumentation

Initial experimentation is performed on polystyrene microspheres. A dilute microsphere suspension is injected into one of the wells of a microchip (shown in Fig. 3a), after the channels (8 and 85 mm long) are filled with a buffer. Through the use of micromachined channels (depth 20 μm, width 50 μm), manipulation of tiny quantities of reagents and samples takes place at much higher speed than macroscopic procedures commonly performed in molecular biology. Sample transfer by manual intervention is eliminated, as well as the need to perform each procedure on a separate instrument.

Micralyne Inc. (Edmonton, Canada) has developed an integrated manipulation unit, the microfluidic toolkit (μTK). A block diagram and detailed presentation of the μTK are given in [12]. In summary, the kit consists of two 6-kV power supplies coupled with a laser-induced fluorescence detection system. The outputs from the high-voltage boards are switched between ground, floating and high-voltage states, and are connected to platinum electrodes in a grid above the microchip stage. A Nd:YAG diode-pumped solid state laser (532 nm) excites the fluorophores in the biological specimens. Fluorescence is collected with a 40×, 0.55 NA objective, and sent toward a photomultiplier tube after deflection by a dichroic mirror. A 10 nm bandpass filter centered at 568.2 nm is placed in the optical path of the photomultiplier tube. The μTK is usually employed for electrophoretic experiments [12]. However, for our current application, we only need to manipulate the polystyrene microspheres to a convenient location in the channels, without inducing fluorescence.

The microspheres move first toward the channel intersection, and then along the other channel until they reach the desired location for detection. The microchip is subsequently removed from the μTK and introduced into the optical detection system. A He-Ne laser illuminates the cell in the channel.

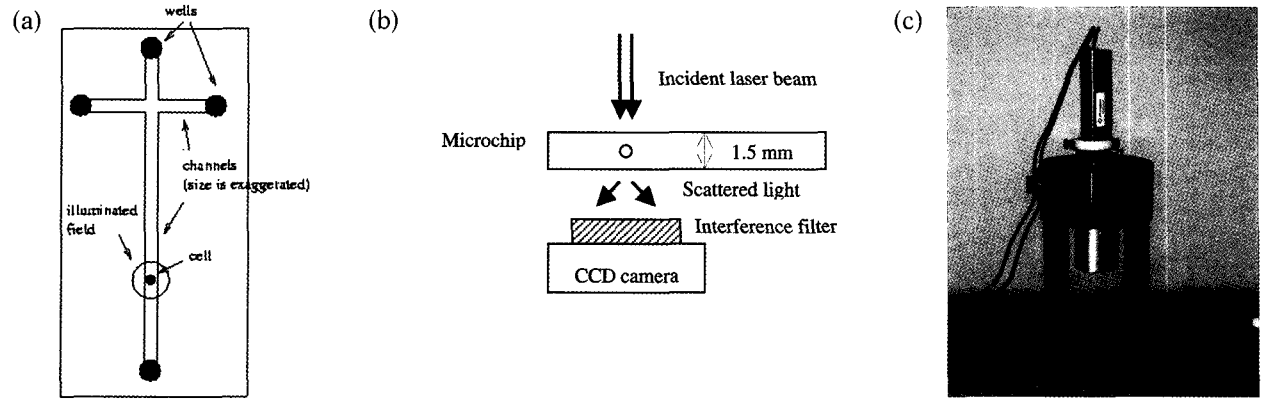

Fig. 3. a) Microchip for manipulation of cells. b) Schematic of the optical system incorporating an interference filter for detecting light scattered by a biological cell or microsphere. c) Picture of the actual device. Camera and filter are contained in the silver barrel.

The scattered light is filtered and recorded by the CCD camera. To be able to record the intensity level of the weaker scattering peaks above ~10°, we estimated a signal-to-noise ratio (SNR) of at least 36 dB is required. Based on the characteristics of Starlight-Xpress HX 516 [20] and on the SNR formula [21]

$$SNR = \frac{IQEt}{\sqrt{IQEt + N_d t + N_r^2}} \tag{7}$$

we chose the mentioned camera for initial experimentation. The parameters in expression (7) define most CCD cameras and correspond to: intensity I (photons/s per pixel), quantum efficiency QE, integration time t (seconds), dark current N_d (electrons/pixel/second), and read noise N_r (electrons rms/pixel) [21].

A simple schematic of the optical detection system incorporating a filter is illustrated in Fig. 3b, whereas Fig. 3c shows a picture of the actual device. The interference filter is attached to the camera contained in the silver barrel (excluding cables). Initial experimentation is performed on polystyrene microspheres of 9.64 μm diameter (Interfacial Dynamics Corporation, Portland, OR, USA). A 1 μL suspension containing approximately 300 microspheres is illuminated by 1 mW of a 632.8 nm He-Ne laser beam with 0.48 mm waist. The refractive index of the microspheres is 1.59. Microspheres are sufficiently separated from each other to prevent superposition of light scattered by individual spheres.

The unscattered light of the laser beam is too strong to permit imaging without a filter. The very sensitive Starlight-Xpress HX 516 camera experiences immediate saturation, even for 100 ms exposure times. A commercial shortwave-pass interference filter of cut-off wavelength 580 nm (Coherent Inc., Santa Clara, CA, USA) is used to significantly attenuate intensity levels below ~10°.

RESULTS AND DISCUSSION

The proposed optical device is intended for single cell analysis. Consequently, using the μTK was necessary to ensure physical separation of the objects subjected to analysis, in this case polystyrene microspheres. Whether a sphere or an actual biological cell, an important step towards obtaining reliable results is to allow detection of individual entities. To this end, it is best if the sample collected for analysis contains as few cells as possible. Furthermore, it should be emphasized that the optical device does not record the image of a cell, but rather its diffraction pattern. Even if the CCD camera images the diffraction patterns of several cells in one picture, the separation between the cells has to be large enough so that the diffraction patterns do not overlap, and each pattern corresponds to a distinct cell. After recording the diffraction patterns of individual cells, the patterns are analyzed separately, and results are subsequently averaged.

Fig. 4a illustrates an optical diffraction pattern of an individual microsphere, *i.e.* a typical image of filtered light scattered over an approximate angular range of 0° to 10°. Although patterns of several spheres were recorded simultaneously, each pattern is analyzed individually. The following discussion explains the mathematical approach that was implemented into the analysis of the recorded diffraction patterns.

The array of squares represents the pixels in a grayscale image. The grayscale data is stored in a two-dimensional (2D) array denoted X. The numbers along the left and lower boundaries of the grayscale image (see Fig. 4a) are row and column indexes, respectively for individual pixels, and directly correspond to how the image data is stored in a conventional matrix. The pixel value is $X(I,J)$, where I is the row index, and J is the column index. The xy-axes are centered at the origin O which is taken as the center of the microsphere in the image. The diameter of the microsphere is slightly larger than a pixel size.

A diffraction pattern of a microsphere has radial symmetry, and so we wish to produce a plot of the average pixel value at some radial distance from O. This involves the need to interpolate the 2D array at various radial distances from O at some specified angle α ($0 \le \alpha < 360°$) with respect to the x-axis. We assume radial distance in increments of one pixel width, and pixels are assumed to

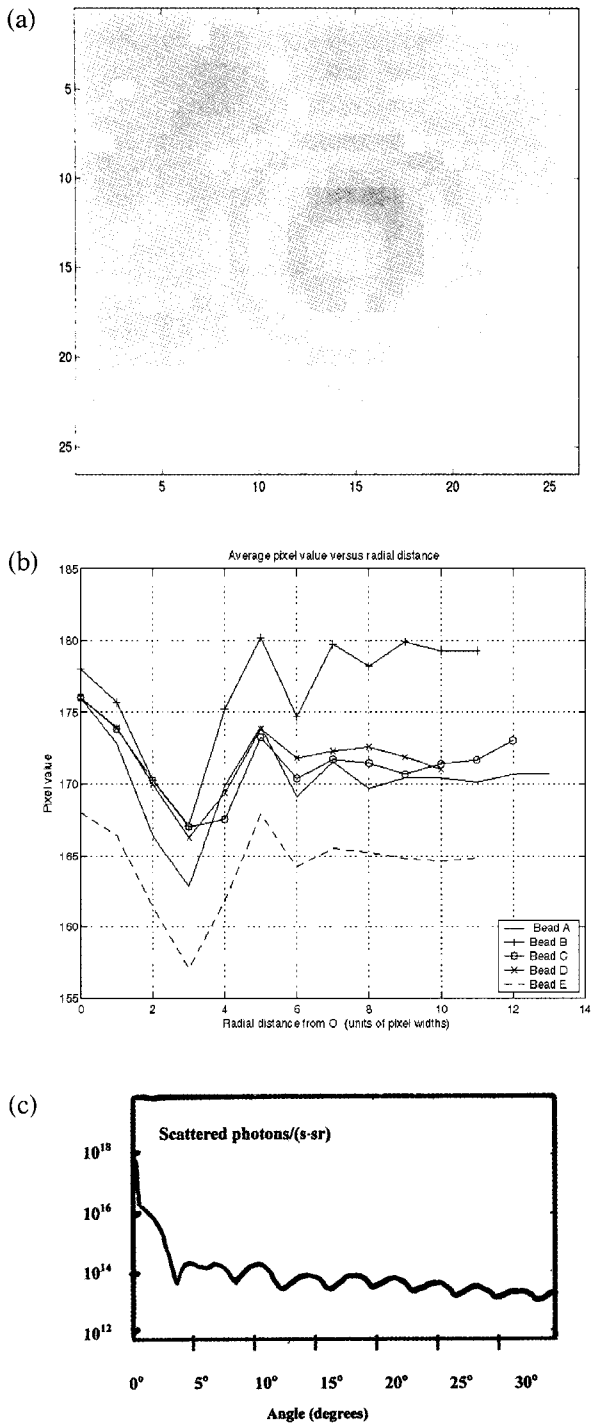

Fig. 4. a) Scattered light (angular range ~0° to 10°) detected by CCD sensor over 10 ms exposure time. CCD sensor pixel size: 7.4 μm × 7.4 μm. Incident beam: He-Ne laser of 632.8 nm. Scattered light originates from polystyrene microspheres of diameter 9.64 μm, refractive index 1.59, immersed in deionized water. b) Average pixel values versus radial distance from the center for five different microspheres. Pixel values are in the range 0 (black) to 255 (white); c) Calculated filtered photon counts.

be one unit in width. Thus, the distance from O at angle α is

$$r_k = k \tag{8}$$

for which $k = 0, 1, \ldots, M-1$; M = pixel number. The pixel value at distance r_o must therefore be $X(IC, JC)$ for all possible α. We need to interpolate the array X for $k = 1, 2, \ldots, M-1$. The Cartesian coordinates of the pixel at angle α, and radial distance r_k from O are

$$X_k = k \cos\alpha \quad , \quad Y_k = k \sin\alpha \tag{9}$$

The value of the pixel at these coordinates is given by $p(k\cos\alpha, k\sin\alpha)$ where the interpolating function $p(x,y)$ is defined by

$$p(x,y) = \sum_{i=0}^{1}\sum_{j=0}^{1} p(x_i, y_j) l_i(x) l_j(y) \tag{10}$$

such that

$$l_j(x) = \prod_{i=0, i\neq j}^{1} \frac{x - x_i}{x_j - x_i} \tag{11}$$

for suitable coordinates (x_i, y_j). These coordinates are the locations of four pixels that form a 2 × 2 square, and such that $x_o \leq X_k \leq x_1$, and $y_o \leq Y_k \leq y_1$. Eq. (10) is a particular case of the 2D Lagrange interpolation procedure suggested in [22]. The procedure was implemented into MATLAB codes, and the diffraction patterns of several microspheres were processed. Fig. 4b illustrates average pixel values for five microspheres for a given radial distance from the center pixel. By comparison, Fig. 4c shows a calculated scattered light distribution for a microsphere. Calculations do not account for scattering off the edges of the microchannel, or absorption in the glass microchip. The unscattered light at 0° is not considered.

The analysis of the recorded optical diffraction patterns shows that the interference filter has managed to sufficiently attenuate intensities in the 0° to 10° range. The thin-film filter peak equalizer is wavelength limited in that the filter is chosen for a particular laser wavelength. If a different laser wavelength is employed, a new filter needs to be designed or purchased, if commercially available. This is not a problem, since the calculations can be redone for a different laser.

The information collected for scattering angles between 0° and 10° may not be sufficient to infer how advanced the disease is in the cell, however, the method discussed above illustrates the principle of enhancing diffraction patterns using thin-film optical filters. The next obvious step in the design of the optical device is to reduce the distance between the scatterer (*i.e.* cell, microsphere *etc.*) and the CCD sensor, thus extending selective peak attenuation to a wider angular range. As discussed in the introduction, a wide angular range will allow collecting enough information about the constituents of the cell and their health.

CONCLUSION

It is known that light scattering and the obtained diffraction patterns can offer reliable diagnostics for diseased cells. Analyzing diffraction patterns over a wide range of angles could resolve morphological differences at the subcellular level. Our work encompasses a proposal for cell analysis through the enhancement of optical diffraction patterns using thin-film optical filters. The novel idea is that the large dynamic range of scattered light intensities from biological cells or similar sized objects could be reduced through selective attenuation. To this purpose, we show that an interference filter can be employed to selectively enhance diffraction peaks. Although the 580 nm shortwave-pass interference filter that we used does not bring all intensity levels to the same height, scattering peaks below ~10° were shown experimentally to be significantly attenuated. In addition, calculations show that reasonable scattering peak equalization for intensities at angles larger than 10° can be obtained.

To enable the design of the optical device and an appropriate filter, an alternative simulation method based on the spectral algorithm is used for calculating scattered light distributions. Simulation results are in good agreement with other more established techniques such as Mie theory. The simulated diffraction patterns were used to verify the experimental data.

Initial experimentation with the new device was performed on polystyrene microspheres. To ensure separation between the analyzed microspheres, sample manipulation was done inside the channels of a microchip inserted in a commercial microfluidic toolkit. By employing an optical device that uses selective enhancement of individual diffraction patterns of cells over large scattering angles, improved data collection may be possible in medical applications. In addition, the compactness and affordability of the proposed optical device may allow wide spread use.

REFERENCES

[1] Vo-Dinh, T., B. M. Cullum, and D. L. Stokes (2001) Nanosensors and biochips: Frontiers in biomolecular diagnostics. *Sens. Actuat. B. Chem.* 74: 2-11.

[2] Mourant, J. R., J. P. Freyer, A. H. Hielscher, A. A. Eick, D. Shen, and T. M. Johnson (1998) Mechanisms of light scattering from biological cells relevant to noninvasive optical-tissue diagnostics. *Appl. Opt.* 37: 3586-3593.

[3] Backman, V., V. Gopal, M. Kalashnikov, K. Badizadegan, R. Gurjar, A. Wax, I. Georgakoudi, M. Mueller, C. W. Boone, R. R. Dasari, and M. Feld (2001) Measuring cellular structure at submicrometer scale with light scattering spectroscopy. *IEEE J. Select. Top. Quant. Electron.* 7: 887-893.

[4] Drezek, R., A. Dunn, and R. Richards-Kortum (1999) Light scattering from cells: Finite-difference time-domain simulations and goniometric measurements. *Appl. Opt.* 38: 3651-3661.

[5] Drezek, R., A. Dunn, and R. Richards-Kortum (2000) A pulsed finite-difference time-domain (FDTD) method for calculating light scattering from biological cells over broad wavelength ranges. *Opt. Express* 6: 147-157.

[6] Schrum, D., C. Culbertson, S. Jacobson, and M. Ramsey (1999) Microchip-flow cytometry using electrokinetic focusing. *Anal. Chem.* 71: 4173-4177.

[7] Altendorf, E. H. and P. Yager (1998) Silicon microchannel optical flow cytometer. *US Patent* 5,726,751.

[8] Canuto, M. Y. Hussaini, A. Quarteroni, and T. A. Zang (1988) *Spectral Methods in Fluid Dynamics*. Springer-Verlag, Berlin, Germany.

[9] Shao, Y., A. V. Maximov, I. G. Ourdev, W. Rozmus, and C. E. Capjack (2001) Spectral method simulations of light scattering by biological cells. *IEEE J. Quant. Electron.* 37: 617-625.

[10] Shao, Y. (2002) *Modeling of Light Propagation in Biological Tissues*. Ph.D. Thesis. University of Alberta, Edmonton, Alberta, Canada.

[11] Amin, M. R., C. E. Capjack, P. Frycz, W. Rozmus, and V. T. Tikhonchuk (1993) Two-dimensional simulations of stimulated Brillouin scattering in laser produced plasma. *Phys. Rev. Lett.* 71: 81-84.

[12] Crabtree, H. J., E. C. S. Cheong, D. A. Tilroe, and C. J. Backhouse (2001) Microchip injection and separation anomalies due to pressure effects. *Anal. Chem.* 73: 4079-4086.

[13] Dunn and R. Richards-Kortum (1996) Three-dimensional computation of light scattering from cells. *IEEE J. Select. Top. Quant. Electron.* 2: 898-905.

[14] Mie, G. (1908) Considerations on the optics of turbid media, especially colloidal metal solutions. *Ann. Phys.* 25: 377-442.

[15] Kohl, M. and M. Cope (1994) Influence of glucose concentration on light scattering in tissue. *Opt. Lett.* 17: 2170-2172.

[16] Dunn (1997) *Light Scattering Properties of Cells*. Ph.D. Thesis. University of Texas at Austin, Austin, Texas, USA.

[17] Stefanita, C.-G., Y. Shao, W. Rozmus, C. E. Capjack, and C. J. Backhouse, Filtering scattered light in microchip-based cell diagnostics *IEEE Trans. Instr. Meas.* (in press).

[18] Interference filter manufacturers' website or product catalogues: *e.g.* Coherent Inc., Andover Corporation, Melles Griot, Oriel *etc.*

[19] Azzam, R. M. A. and N. M. Bashara (1977) *Ellipsometry and Polarized Light*. North Holland.

[20] Starlight Xpress (2002), available online: http://www.starlightccd.com

[21] Roper Scientific (2002), available online: http://www.roperscientific.com/library_enc_signal.shtml

[22] Quarteroni, A., R. Sacco, and F. Saleri (2000) *Numerical Mathematics* (Texts in Appl. Math., Vol. 37). Springer Verlag, New York, USA.

[Received July 2, 2004; accepted November 5, 2004]